

Effect of CO₂-induced ocean acidification on the early development and shell mineralization of the European abalone (*Haliotis tuberculata*)

Wessel Nathalie ^{1, 2}, Martin Sophie ^{3, 8}, Badou Aicha ¹, Dubois Philippe ⁴, Huchette Sylvain ⁵, Julia Vivien ^{1, 6}, Nunes Flavia ^{6, 7}, Harney Ewan ⁶, Paillard Christine ⁶, Auzoux-Bordenave Stéphanie ^{1, 8, *}

¹ MNHN CNRS IRD UPMC, Stn Biol Marine Concarneau, Museum Natl Hist Nat, UMR 7208, Biol Organismes & Ecosyst Aquat BOREA, F-29900 Concarneau, France.

² IFREMER, Dept Oceanog & Dynam Ecosyst ODE, Rue Ile Yeu, BP21105, F-44311 Nantes 3, France.

³ Stn Biol Roscoff, AD2M, UMR 7144, F-29680 Roscoff, France.

⁴ Univ Libre Bruxelles, Lab Biol Marine, CP160-15, B-1050 Brussels, Belgium.

⁵ Ecloserie France Haliotis, F-29880 Kerazan, Plouguerneau, France.

⁶ UEB, Univ Brest UBO, Lab Sci Environm Marin LEMAR, UMR 6539 CNRS UBO IRD Ifremer, Inst Univ Europeen, Pl Nicolas Copernic, F-29280 Plouzane, France.

⁷ IFREMER, Ctr Bretagne, DYNÉCO, Lab Coastal Benth Ecol LEBCO, F-29280 Plouzane, France.

⁸ Sorbonne Univ, 4 Pl Jussieu, F-75005 Paris, France.

* Corresponding author : Stéphanie Auzoux-Bordenave, email address :
stephanie.azoux-bordenave@mnhn.fr

Abstract :

Ocean acidification is a major global stressor that leads to substantial changes in seawater carbonate chemistry, with potentially significant consequences for calcifying organisms. Marine shelled mollusks are ecologically and economically important species providing essential ecosystem services and food sources for other species. Because they use calcium carbonate (CaCO₃) to produce their shells, mollusks are among the most vulnerable invertebrates to ocean acidification, with early developmental stages being particularly sensitive to pH changes. This study investigated the effects of CO₂-induced ocean acidification on larval development of the European abalone *Haliotis tuberculata*, a commercially important gastropod species. Abalone larvae were exposed to a range of reduced pHs (8.0, 7.7 and 7.6) over the course of their development cycle, from early-hatched trophophore to pre-metamorphic veliger. Biological responses were evaluated by measuring the survival rate, morphology and development, growth rate and shell calcification. Larval survival was significantly lower in acidified conditions than in control conditions. Similarly, larval size was consistently smaller under low pH conditions. Larval development was also affected, with evidence of a developmental delay and an increase in the proportion of malformed or unshelled larvae. In shelled larvae, the intensity of birefringence decreased under low pH conditions, suggesting a reduction in shell mineralization. Since these biological effects were observed for pH values expected by 2100, ocean acidification may have potentially negative consequences for larval recruitment and persistence of abalone populations in the near future.

Highlights

► Calcifying mollusks are among the most vulnerable invertebrates to (OA). ► Early life-history stages are particularly sensitive to pH changes. ► We investigated the effects of OA on larval development of the abalone *H. tuberculata*, a commercially important gastropod. ► Larval survival, development and shell calcification were affected by low pH conditions. ► OA may have potentially negative consequences for larval recruitment and persistence of abalone populations.

Keywords : Ocean acidification, Abalone, Larval development, Shell mineralization

50 **1. Introduction**

51 Ocean acidification and warming are major concerns for marine ecosystems. By the
52 end of the 21st century, global mean surface temperatures are expected to increase by 1
53 to 3°C, while surface ocean pH is likely to decrease by 0.1 to 0.3 units (Gattuso et al.,
54 2015). These changes will lead to alterations in seawater carbonate chemistry and a
55 reduction in the degree of saturation with respect to calcium carbonate (Gattuso et al.,
56 2015; IPCC, 2014). Since marine benthic ecosystems constitute a reservoir for
57 biodiversity, several studies have focused on the evaluation of changing ocean
58 conditions on marine biodiversity via the measurement of key physiological and
59 ecological processes in marine organisms (for a review, see Widdicombe and Spicer,
60 2008).

61 Changing ocean conditions are considered as major threats to marine species,

affecting early development, skeletal growth and key physiological functions, which can ultimately impact animal behaviour and species distribution (Kroeker et al., 2010; Widdicombe and Spicer, 2008). Reduced oceanic pH has been shown to impact a variety of calcifying species, such as corals, mollusks and echinoderms, leading to contrasting biological responses (Hendricks et al., 2010; Hofmann et al., 2010; Wittmann and Pörtner, 2013). Because calcium carbonate (CaCO_3) is necessary for shell production, mollusks are among the most vulnerable invertebrates to ocean acidification, with larval and juvenile stages being particularly vulnerable (Gazeau et al., 2013; Orr et al., 2005; Przeslawski et al., 2015 Talmage and Gobler, 2010). Indeed, it is during larval development that marine mollusks initiate the deposition of calcium carbonate (CaCO_3) to build their shell (Kurihara, 2008).

A number of studies have reported delays in development, reduced growth rate and/or shell abnormalities in larval mollusks that could potentially affect larval survival, metamorphosis and recruitment into adult populations (Parker et al., 2013; Ross et al., 2011). The impacts of ocean acidification may be particularly severe for bivalves and gastropods, which start to calcify at early developmental stages (Parker et al., 2013). Since many mollusk species are commercially important food sources, negative impacts of ocean acidification may also result in significant economic loss (Ekstrom et al., 2015; Gazeau et al., 2007). Several studies have recently focused on the impacts of elevated partial pressure of CO_2 ($p\text{CO}_2$) on embryonic and larval stages of shelled mollusks, especially cultivated bivalves (see reviews by Gazeau et al., 2013; Parker et al., 2013). In comparison to marine bivalves, our knowledge of the impacts of elevated $p\text{CO}_2$ on early developmental stages in gastropods is based on fewer studies, covering only about four genera (*Cavolinia*, *Crepidula*, *Littorina* and *Haliotis*). In the gastropods studied to date, ocean acidification was shown to reduce larval survival, increase development time, alter morphology and/or impair shell formation and calcification (Byrne et al.,

88 2011; Comeau et al., 2010; Crim et al., 2011; Ellis et al., 2009; Guo et al., 2015; Kimura
89 et al., 2011; Noisette et al., 2014; Zippay and Hofmann, 2010).

90 Among the species that have been considered in acidification studies, abalone
91 (*Haliotis* spp.) are ecologically and economically important, acting as grazers in the
92 marine ecosystem and as a food source for humans (Cook, 2014; Huchette and Clavier,
93 2004). Many abalone species worldwide have experienced severe population declines
94 due to both overfishing and the combined effects of environmental stressors such as
95 elevated CO₂, global warming and pathogen occurrence (Crim et al., 2011; Travers et
96 al., 2009; Morash and Alter, 2015). Early-life-history stages of abalone appear to be
97 negatively affected by elevated CO₂, with a higher percentage of deformed larvae under
98 low pH conditions than other intertidal marine mollusks such as oysters (Byrne et al.,
99 2011; Crim et al., 2011; Guo et al., 2015; Kimura et al., 2011; Zippay and Hofmann,
100 2010). For example, elevated seawater CO₂ concentrations impaired larval development
101 and reduced larval survival in the northern abalone *Haliotis kamtschatkana* (Crim et al.,
102 2011). In the abalone *H. coccoradiata*, embryos were dramatically affected by a
103 combination of warm (+2 to +4°C) and acidified conditions (-0.4 to -0.6 pH units) with
104 only a small percentage surviving, and with those embryos that did survive producing
105 unshelled larvae (Byrne et al., 2011).

106 The European abalone *Haliotis tuberculata* is a commercially important mollusk
107 species, for which the whole life cycle is completed under anthropogenic control
108 (Courtois de Viçose et al., 2007). As for most marine invertebrates, abalone display a
109 pelago-benthic life cycle with a larval planktonic stage followed by a critical
110 metamorphosis into the benthic juvenile, making them highly sensitive to environmental
111 changes (Byrne et al., 2011). Larval development and shell formation have been
112 extensively studied in *H. tuberculata*, with deposition of amorphous calcium carbonate
113 (ACC) in the early larval shell followed by deposition of aragonite in the juvenile and

114 adult shell (Auzoux-Bordenave et al., 2010). Since ACC and aragonite are relatively
115 soluble forms of CaCO₃ (compared to calcite), the abalone shell is a relevant model for
116 investigating the effects of ocean acidification. The controlled production of *Haliotis*
117 *tuberculata* embryos and larvae provides a unique opportunity to study the impact of
118 acidification on the early development of a marine calcifying species.

119 Here we investigated the effects of CO₂-induced ocean acidification on survival,
120 early development, growth and shell mineralization during the entire larval development
121 of the European abalone *Haliotis tuberculata*. Abalone larvae, obtained from a
122 controlled fertilization carried out at the 'France-Haliotis' hatchery, were exposed to
123 three experimental pHs (8.0, 7.7 and 7.6) throughout their larval development.
124 Biological responses of larvae were evaluated by measuring the survival rate,
125 morphology and development, growth and shell calcification. Optical and SEM
126 microscopy analyses were performed to assess whether reduced pH had an influence on
127 larval shell morphology and microstructure.

128

129 **2. Materials and methods**

130

131 **2.1. Production of abalone larvae**

132 *Haliotis tuberculata* parental stock were collected from northwest Brittany (Roscoff,
133 France) and conditioned in flowing seawater at the 'France-Haliotis' commercial
134 abalone hatchery (Plouguerneau, France). Larvae were obtained from controlled
135 fertilizations carried out in September 2013 at a water temperature of 17.0 ± 0.5°C,
136 which led to approximately 6x10⁶ larvae. Following fertilization, egg density was
137 evaluated under a binocular microscope and the embryos were transferred to
138 experimental tanks for acidification experiments.

139 **2.2. Experimental design**

140 The effects of lowered pH were investigated by exposing abalone larvae to three pH
141 conditions, including one present-day control pH 8.0 ($p\text{CO}_2 \approx 400 \mu\text{atm}$) and two levels
142 of pH predicted under varying climate change scenarios: 7.7 ($p\text{CO}_2 \approx 1000 \mu\text{atm}$) and
143 7.6 ($p\text{CO}_2 \approx 1400 \mu\text{atm}$), as outlined by Riebesell et al. (2010). Experiments were carried
144 out in September 2013 at the ‘France-Haliotis’ hatchery, according to an experimental
145 design adapted from Martin et al. (2011). Fertilized embryos were grown in 300 L tanks
146 of flowing seawater at a density of 5×10^5 per tank, under the three $p\text{CO}_2$ conditions, and
147 with two replicate tanks per condition. The effects of seawater acidification were
148 investigated over the total duration of larval development (5 days), from early-hatched
149 trochophore larvae to the pre-metamorphic stage. *Haliotis* larvae are lecithotrophic and
150 were not fed during the experiment, avoiding any influence of diet on the biological
151 responses.

152

153 *2.2.1. pH control and carbonate chemistry*

154 Larval tanks were kept in a temperature-controlled room and supplied with natural
155 filtered seawater that was continuously aerated with ambient air. The temperature and
156 salinity were measured daily using a conductimeter (3110, WTW, Germany). Low
157 seawater pH was obtained by bubbling CO₂ (Air liquide, France) into the tanks through
158 electro-valves regulated by a pH-stat system (Aquastar, IKS Computer System,
159 Germany). Seawater pH (pH_T, expressed on the total hydrogen ion concentration scale,
160 Dickson, 2010) was adjusted to the desired level from ambient pH_T (8.0) to low pH_T
161 (7.7 and 7.6) to within ± 0.05 pH units. pH values on the National Bureau of Standards
162 (NBS) scale obtained with the pH-stat system were adjusted daily with measurements of
163 pH_T for each tank using a pH meter (Metrohm 826 pH mobile, Metrohm, Switzerland)

164 with a glass electrode (Metrohm electrode plus) calibrated on the total scale using
165 Tris/HCl and 2-aminopyridine/HCl buffer (Dickson *et al.*, 2007). pH (NBS) was
166 recorded every 15 minutes in each tank by the pH-stat system and converted to pH_T by
167 using daily measurements.

168 Total alkalinity (A_T) of seawater was measured twice on 100 ml samples taken from
169 incoming water and from each experimental tank. Seawater samples were filtered
170 through 0.7 µm Whatman GF/F membranes, immediately poisoned with mercuric
171 chloride and stored in a cool dark place pending analyses. A_T was determined
172 potentiometrically using an automatic titrator (Titroline alpha, Schott SI Analytics,
173 Germany) calibrated with the National Bureau of Standards scale. A_T was calculated
174 using a Gran function applied to pH values ranging from 3.5 to 3.0 as described by
175 Dickson *et al.* (2007) and corrected by comparison with standard reference material
176 provided by Andrew G. Dickson (CRM Batch 111). pCO₂ and other parameters of
177 carbonate chemistry were determined from pH_T, A_T, temperature and salinity by using
178 the CO₂SYS software (Lewis and Wallace, 1998) using constants from Mehrbach *et al.*
179 (1973) refitted by Dickson and Millero (1987).

180

181 *2.2.2. Larval sampling and measurements*

182 Larval development was monitored by daily observations with a binocular
183 microscope. Larvae were sampled at four different development stages: trochophore
184 (approximately 20 hours post fertilization, hpf), early veliger (30 hpf), post-torsional
185 veliger (48 hpf) and pre-metamorphic stage (96 hpf). At each sampling time point, 10-
186 12 L of seawater containing larvae were collected from each tank. Larval viability was
187 calculated at each stage as the proportion of live larvae divided by the total number of
188 larvae (n ≈ 200). Larvae were filtered on a 40 µm-sieve and aliquoted into 15 ml tubes.
189 Larval samples were then fixed in either 70% ethanol for transmitted and polarized light

190 microscopy or in a 3% glutaraldehyde solution in Sörensen-sucrose buffer, adjusted to
191 1100 mOsm for SEM analysis.

192

193 **2.3. Light and polarized microscopy**

194 *2.3.1. Slide preparation and observation*

195 Microscopic slides were prepared with ethanol-fixed larvae from the different pH
196 conditions (two slides per condition). Approximately 100 larvae were whole-mounted in
197 a drop of glycerol, with the amount of ethanol transferred kept to a minimum. Slides
198 were kept at room temperature for 5 to 10 min, allowing ethanol to evaporate and larvae
199 to settle. Four spots of vacuum gel were deposited on the corners of a squared cover slip
200 to prevent the larvae being crushed. After placing the cover slip over the glycerol, the
201 slides were gently sealed with varnish. About 200 larvae per condition were observed
202 and photographed under phase contrast and polarized light with an Olympus binocular
203 microscope (Olympus, Hamburg, Germany) equipped with polarizing filters. All images
204 were acquired with a digital camera (DS-Ri1, Nikon) at 100x magnification and 40 ms
205 light exposition. Images were analyzed with NIS-element and Image-J software.

206

207 *2.3.2. Morphometrical analysis*

208 Larval development stage, shell presence and size were determined under light
209 microscopy ($n = 100$ larvae per tank, 200 larvae per pH condition). Maximal larval
210 length and width of normal larvae were measured in specimens lying on the lateral side,
211 as shown by the dotted black arrows in Figure 1. The product of length * width was
212 calculated for each larva and the mean of these values per tank was computed. A growth
213 index per tank was calculated as the square root of each of these means.

214 Trochophore larvae were scored as one of four possible morphological groups,
215 according to the presence/absence of larval shell, the occurrence of body abnormalities
216 and/or delayed development:

217 1- normal shelled larvae (Fig 1A),

218 2- shelled larvae with abnormalities or delayed development,

219 3- unshelled larvae with normal body (Fig 1B),

220 4- unshelled larvae with abnormalities or delayed development,

221 For veliger stages, the presence/absence of shell, body abnormalities and/or delayed
222 development were also recorded. Additional attributes like mantle formation,
223 appearance of eyes or tentacles, and shell abnormalities were included for the
224 assessment of morphological status.

225 According to these parameters, veliger larvae were scored as one of the following four
226 morphological groups:

227 1- normal shelled larvae (Fig. 2A, D, G)

228 2- larvae with shell malformation (Fig. 2B, E)

229 3- larvae presenting body abnormalities or delayed development (Fig. 2H)

230 4- larvae with both shell and body abnormalities (Fig. 2C, F, I)

231

232 *2.3.3. Birefringence analysis*

233 The degree of CaCO₃ mineralization within the larval shell was evaluated by
234 measuring the intensity of birefringence under cross-polarized light using an Olympus
235 microscope, according to the method described by Jardillier et al. (2008). Cross-
236 polarized light passing through calcium carbonate (an anisotropic material) is double
237 refracted. As shells with higher calcium carbonate content double refract more light, the
238 intensity of birefringence can be used as a proxy for the evaluation of shell

239 mineralization (Noisette et al., 2014). Measurements were obtained for 30, 48 and 96
240 hpf larvae. Earlier larval stages were not considered because their shell lacked sufficient
241 crystallized CaCO₃ to calculate birefringence. Birefringence was determined for 40
242 larvae per treatment using Image J software. The mean of grey-scale level (in pixels)
243 was determined for each area of the larval shell showing birefringence (1 to 3 areas per
244 larval shell). The values for each area were averaged into a global mean grey-scale
245 value, providing the birefringence intensity (in %) for each larval shell (Fig S1,
246 electronic supplementary material). Larvae were categorized as one of three types: fully
247 mineralized (birefringence > 90%); partially mineralized (70% < birefringence < 90%)
248 and less mineralized (birefringence < 70%). Finally, the birefringence intensity of larval
249 shells grown under the different pH conditions was expressed as a percentage of larvae
250 distributed in the three categories for each developmental stage.

251

252 **2.4. Scanning electron microscopy (SEM)**

253 Four individuals per pH condition were used for SEM analysis. Larval samples were
254 fixed in a 3% glutaraldehyde solution and then washed in Sörensen-sucrose buffer.
255 Samples were subsequently dehydrated in a series of increasingly concentrated ethanol
256 solutions and were critical point dried with liquid carbon dioxide. Finally, samples were
257 carbon-coated and observed at the “Plateforme d’Imagerie et de Mesures en
258 Microscopie” (PIMM, Université de Bretagne Occidentale, Brest, France) with a
259 scanning electron microscope operating at 5 kV (Hitachi S-3200N).

260

261

262 **2.5. Statistical analyses**

263 All statistical analyses were performed with R software (R Development Core Team,
264 2014) or Systat 12. In order to determine if larval viability was significantly different
265 between pH treatments, an unpaired Student's t-test with Welch correction was
266 performed. For morphological and developmental data, a homogeneity χ^2 test was
267 performed in order to evaluate the effect of elevated $p\text{CO}_2$ on larval phenotypes.
268 Correlation between larval length and width across pH treatments was assessed using a
269 Spearman's correlation test, allowing length and width to be combined as one parameter
270 to estimate growth. Differences in larval growth across pH treatments were assessed by
271 repeated measures ANOVA using the growth index per tank (pH: fixed crossed factor,
272 time: fixed repeated factor) followed by post-hoc Tukey tests for multiple comparisons
273 using the appropriate mean square error (Doncaster and Davey, 2007). To test the effect
274 of pH on shell birefringence, a homogeneity χ^2 test was performed followed by a pair-
275 wise Wilcoxon rank sum. For all tests, differences were considered significant at $p <$
276 0.05.

277 **3. Results**

278 **3.1. Seawater parameters**

279 Mean values of seawater carbonate chemistry parameters are reported in Table 1.
280 The pH_T of experimental aquaria was maintained closed to nominal values throughout
281 the experiment, respectively at a $\text{pH}_T = 8.0$ ($p\text{CO}_2$ of $460 \mu\text{atm} \pm 3\mu\text{atm}$), $\text{pH}_T = 7.68$
282 ($p\text{CO}_2$ of $1055 \pm 3\mu\text{atm}$) and $\text{pH}_T = 7.58$ ($p\text{CO}_2$ of $1331 \pm 10\mu\text{atm}$). In the following
283 sections, rounded mean pH_T values are used namely pH 8.0, 7.7, and 7.6). The
284 temperature was maintained at $17.0 \pm 0.5^\circ\text{C}$ ($n = 5$) and salinity at 37.0 ± 0.1 ($n = 5$) in
285 all tanks and there were no significant differences across treatments. Total alkalinity

286 (A_T) measured from incoming water and from experimental tanks differed only slightly
287 and remained stable over the experiment (mean = 2344 $\mu\text{Eq}.\text{kg}^{-1}$).

288

289 **3.2. Larval viability**

290 Larval viability was measured for the three development stages in the different pH
291 conditions (Fig. 3). In control seawater (pH 8.0) larval viability remained > 95% until
292 the pre-metamorphic stage. A significant decrease in larval viability was observed in
293 reduced pH treatments. At pH 7.7 reduced larval viability was observed in 30 and 48
294 hpf larvae, although the decrease was not significant ($p = 0.257$ and $p = 0.125$
295 respectively), but a 50% reduction in viability at 96 hpf was significant (unpaired
296 Student's t-test, $p < 0.001$). At pH 7.6, viability slightly decreased to 75% at 30 hpf ($p =$
297 0.067) and dropped to 56% and 47% at 48 and 96 hpf respectively (unpaired Student's t-
298 test, $p = 0.001$ and $p = 0.008$ respectively). Abnormalities in larval morphology and
299 hyperactive movements were observed in the two low pH conditions for all four larval
300 stages (S. Auzoux-Bordenave, pers. observations).

301 **3.3. Morphology and development**

302 Larval developmental stage and shell presence were determined at each time point
303 and compared between the different treatments, according to the four morphological
304 groups defined in section 2.3.2. Larval distribution within these groups across the
305 different pH treatments is shown for the trochophore stage (Fig. 4A) and later veliger
306 stages (Figs. 4B-D). At each developmental stage, conformity χ^2 tests showed that the
307 distribution within the groups was dependent on the pH ($p < 0.001$).

308 At the first developmental stage (20 hpf trochophore), larval distribution into the
309 different morphological groups was pH dependent (Fig. 4A; $\chi^2 = 83.31$, df = 6, $p <$

310 0.001). Normal shelled larvae represented 60% of the total amount of larvae in the
311 control group, while this proportion was less than 10% at the lowest pH ($\chi^2 = 83.31$, df =
312 6, $p < 0.001$). The percentage of shelled larvae, including those with normal and
313 abnormal bodies, was significantly lower at pH 7.6 (47%) compared to controls (75%)
314 ($\chi^2 = 25.19$, df = 2, $p < 0.001$). In parallel, the percentage of unshelled larvae was
315 significantly greater at pH 7.6 (53%) compared to controls (10%) ($\chi^2 = 25.19$, df = 2, $p <$
316 0.001). The presence of unshelled larvae with normal bodies in the control group
317 probably occurred due to differences in the timing of shell morphogenesis among
318 individuals.

319 The distribution of veliger stages into the different morphological groups was also
320 pH dependent, and similar to that observed in trochophore larvae (Fig. 4B-D). At 30
321 hpf, a strong decrease in the percentage of normal larvae was observed, from 60% in the
322 control group to only 10% at the lowest pH (Fig. 4B; $\chi^2 = 75.25$, df = 6, $p < 0.001$).
323 Meanwhile, the proportion of malformed or delayed larvae increased from 25 to 45%.
324 An important impact of acidification was observed at 48 hpf, where the proportion of
325 normal larvae decreased from 90% in the control condition to about 58% at pH 7.7 and
326 less than 20% at pH 7.6. (Fig. 4C; $\chi^2 = 133.77$, df = 6, $p < 0.001$). The proportion of
327 larvae showing both shell and body abnormalities (cumulative effects) strongly
328 increased when pH was reduced, from a negligible percentage in the control group, to
329 above 65% at pH 7.6 ($\chi^2 = 133.77$, df = 6, $p < 0.001$). At 96 hpf, the percentage of
330 normal larvae also drastically decreased in the reduced pH treatments, from 70% in the
331 control group to 25% at pH 7.7 and to 12% at pH 7.6 (Fig. 4D) ($\chi^2 = 119.14$, df = 6, $p <$
332 0.001). As a result, the amount of larvae with body malformations or delayed
333 development increased significantly with seawater acidification, from 20% in control
334 conditions to 45% at pH 7.6. For all three veliger stages, the proportion of larvae that
335 showed both shell and body abnormalities (cumulative effects) strongly increased when

336 lowering the pH, while the proportion of larvae displaying only shell malformation
337 remained < 15% and did not differ significantly among treatments.

338 Larval shells (48 hpf) grown at lower pH exhibited differences in the texture and
339 porosity of the surface layer (Fig. 5). In control larvae, the mineralized protoconch
340 almost completely covered the larval body (Fig. 5A). At higher magnification, the shell
341 surface showed a uniform granular texture covered by a very thin homogeneous layer
342 (Fig. 5B). In 48 hpf veliger larvae exposed to decreased pH (7.6), the protoconch
343 exhibited an irregular surface, with differences in thickness, and the homogeneous outer
344 layer was not as distinct as that of control larvae (Fig. 5C). The outer surface had a
345 porous appearance with numerous small holes interspaced between the biominerals and
346 remnants of the organic coating (Fig 5.D).

347

348 **3.4. Larval growth**

349 Length and width of abalone larvae reared in the three pH conditions were measured.
350 Only normal larvae were used in order to determine if growth rate differed according to
351 pH. For each treatment, a Spearman's correlation was carried out to evaluate the
352 relationship between larval length and width during the course of the experiment (Table
353 2). The results showed a linear relationship between the two measures for each pH
354 group (Fig. 6), allowing length and width to be combined as one parameter to estimate
355 larval growth. The growth index (calculated as the square root of length * width) of
356 larvae exposed to the three pH conditions and according to time is presented in Figure
357 7.

358 Both pH and time significantly affected the growth index (Table 3A; $p = 0.009$ and p
359 < 0.001 , respectively), while the interaction term was not significant (Table 3A; $p =$
360 0.088). Larval size significantly increased between 20 hpf and 30 hpf and between 48

361 hpf and 96 hpf (Table 3B; Tukey, $p = 0.002$ and $p = 0.009$, respectively). Larval size
362 was significantly lower at pH 7.7 and 7.6 vs 8.0 (Tukey, $p = 0.008$ and $p = 0.031$,
363 respectively) but did not differ significantly between the two low pH treatments (Table
364 3B; Tukey, $p = 0.105$).

365

366 **3.5. Shell calcification**

367 Under control pH conditions, larvae clearly exhibited the characteristic dark cross
368 indicating a radial arrangement of the aragonite crystals within 2 to 3 areas of
369 birefringence (Fig. 8B). Larvae grown at lower pH (7.6) typically showed a decrease in
370 shell birefringence indicating reduced calcification (Fig. 8D). At 30 hpf, the distribution
371 of larvae into the three categories (i.e. fully mineralized, partially mineralized and less
372 mineralized) was not significantly different between the three pH treatments (Fig. 9A;
373 Table 4A, $\chi^2 = 9.28$, df = 4 , $p = 0.055$). At 48 hpf, the number of fully mineralized
374 larvae was strongly reduced at low pH conditions, while the number of partially and less
375 mineralized larvae was significantly higher (Fig. 9B; Table 4B, $p < 0.001$). Similar
376 results were observed in 96 hpf larvae, with significant differences in larval
377 birefringence between the control group and the low pH group 7.7. (Fig. 9C; Table 4B,
378 $p < 0.001$). At pH 7.6, larval distribution within the three categories was close to that
379 observed in the control group (Table 4B, $p = 0.073$).

380 **4. Discussion**

381 This study provides the first evidence that decreased pH negatively impacts
382 survival, early larval development and shell calcification in the European abalone
383 *Haliotis tuberculata*. Biological responses were measured over the total duration of
384 larval development (from early-hatched trochophore to the pre-metamorphic stage),
385 using near-future oceanic CO₂ levels. Our results are consistent with previous studies on
386 mollusk larvae, in which near-future CO₂ concentrations reduced survival and impaired
387 early development, suggesting potential negative consequences for larval recruitment
388 and the persistence of abalone populations (see reviews by Gazeau et al., 2013; Ross et
389 al., 2011).

390 Our results showed that *H. tuberculata* experienced a significant decrease in larval
391 survival at pH 7.7 and 7.6 with a maximum decrease of 47% at pH 7.6 relative to the
392 control. Furthermore, low pH conditions negatively affected larval morphology, inducing
393 a developmental delay and a decrease in the proportion of shelled larvae. In addition to
394 developmental delays and body abnormalities, seawater acidification resulted in
395 decreased growth rate (length and width). These results are consistent with previous
396 studies on other abalone species, such as those of Byrne et al. (2011), Crim et al. (2011)
397 and Kimura et al. (2011) that found reduced survival in, respectively, *H. coccoradiata*,
398 *H. kamtschatkana* and *H. discus hannai*. Moreover, these studies showed similar results
399 with respect to increasing numbers of unshelled larvae at lower pHs (Byrne et al., 2011;
400 Crim et al., 2011), as well as reduction in larval size (Crim et al., 2011; Kimura et al.,
401 2011). Abalone appears to be particularly sensitive to ocean acidification at early life
402 stages, which may lead to lower recruitment in these commercially and ecologically
403 important species. Similarly, a recent comparison of two abalone species (*H. discus*
404 *hannai* and *H. diversicolor*) together with the oyster *Crassostrea angulata* found

405 reduced size to be a common response to reduced pH (Guo et al., 2015). Among other
406 species, deformities have been observed in the gastropod *Crepidula fornicata* under
407 reduced pH (Noisette et al., 2014), and the oysters *Crassostrea gigas* and *Saccostrea*
408 *glomerata* displayed reduced development rates and increasing levels of abnormalities
409 in low pH treatments (Kurihara et al., 2007; Kurihara, 2008; Parker et al., 2009;
410 Timmins-Schiffman et al., 2013; Watson et al., 2009). More generally, it seems that
411 reduced survival, abnormal or prolonged development and reduced size represent a
412 common response of many marine mollusk larvae exposed to elevated CO₂ (Gazeau et
413 al., 2013; Ross et al., 2011).

414 In addition to reduced survival, development abnormalities and decreased growth
415 rate, seawater acidification also resulted in reduced shell calcification of abalone larvae,
416 as shown by the decrease in birefringence intensity under cross-polarized light. The
417 reduction in shell calcification in larvae grown at lower pH treatments was highly
418 significant at later stages (48 and 96 hpf). However, only a slight, but not significant,
419 increase in the percentage of partially mineralized shells was observed at 30 hpf under
420 low pH 7.7, and no significant differences were observed between control and pH 7.6.
421 This could be related to low amounts of calcium carbonate in the earliest larval shell,
422 which in combination with heterogeneous crystalline orientation, might have resulted in
423 higher variability in the grey levels. In the future, attempts to calibrate grey scale levels
424 with measures of shell mass may allow improvements in the use of birefringence as a
425 proxy for determining shell mineralization.

426 Cross-polarized light and SEM observations of shelled larvae provided evidence of
427 a lack of calcification under lower pH, suggesting that larvae deposited less calcium
428 carbonate and produced a thinner shell. The impacts of ocean acidification on shell
429 calcification have been well studied in juvenile and adult mollusks, showing that their

430 calcified shell is highly sensitive to elevated $p\text{CO}_2$ (Gazeau et al., 2013). For example,
431 in the marine bivalves *Mytilus edulis* and *C. gigas*, the calcification rate was negatively
432 impacted by a short-term exposure to low pH (-0.2 units from ambient, Gazeau et al.,
433 2007). Previous studies have reported a decrease in shell size and shell thickness as well as
434 changes in morphology and shape of the larval shell under elevated $p\text{CO}_2$ (Gazeau et al.,
435 2010; Kurihara et al., 2007, 2008; Miller et al., 2009; Talmage and Gobler, 2009). Few
436 studies have reported changes in larval shell calcification under OA stress by measuring
437 birefringence intensity; however, our results on larval abalone shell are consistent with
438 those of Kurihara *et al.* (2007) and Noisette *et al.* (2014), obtained respectively in
439 *Crassostrea gigas* and *Crepidula fornicata*, showing a reduction in larval shell
440 calcification when seawater pH is lowered.

441 Mollusk shell formation is a complex process starting at the trochophore stage in
442 abalone. The larval shell is formed by a specialized group of ectodermal cells that form
443 the shell gland and the organic periostracum. Primary mineralization takes place
444 between the shell gland and the periostracum, producing the so-called protoconch in
445 gastropods (Eyster, 1986). In abalone, the first deposition of CaCO_3 occurs at an early
446 veliger stage with the deposition of amorphous calcium carbonate (ACC), which is rapidly
447 transformed into crystalline aragonite (Auzoux-Bordenave et al., 2010). Since ACC and
448 aragonite are more soluble forms of CaCO_3 than calcite in lower pH conditions, the larval
449 shell is likely to be more susceptible to dissolution than juvenile or adult shell. In the
450 present study, SEM images of larval shells reared at pH 7.6 revealed numerous small
451 holes at the shell surface, suggesting that CaCO_3 dissolution is likely to be a factor
452 explaining reduced calcification in abalone larvae experiencing acidified conditions.
453 Shell dissolution processes may arise as a result of a lower availability of carbonate ions at
454 the site of calcification (a direct effect of the carbonate chemistry) or through indirect

455 physiological changes in ionic composition, matrix protein formation or enzymatic
456 activities (Hüning et al., 2012).

457 Recent studies have suggested that lowered aragonite saturation state may be one of the
458 key parameters controlling whether shell development in larval mollusks occurs normally
459 (Thomsen et al., 2015; Waldbusser et al., 2015). In the oyster *C. gigas*, developmental
460 success and growth rates were not significantly altered as long as carbonate ion
461 concentrations were above aragonite saturation levels, but they strongly decreased when
462 carbonate ion concentrations dropped below aragonite saturation levels (Gazeau et al.,
463 2011). The authors suggested that the mechanisms used by oyster larvae to regulate
464 calcification rates were not efficient enough to compensate for the low availability of
465 carbonate ions under acidified conditions. Interestingly, recent studies suggest that initial
466 shell formation in larvae can occur even when aragonite is reduced below saturation levels
467 (Frieder et al., 2016), and that dissolution of the initial shell, at least in species such as *M.*
468 *edulis*, only occurs at very high levels of OA (Ramesh et al., 2017). However, it is likely
469 that resource allocation trade-offs between biomineralization and other vital biological
470 processes will begin to occur as larval development progresses, as shown in sea urchins
471 (Pan et al., 2015). This could help to explain why reduced birefringence of *H. tuberculata*
472 larvae under elevated $p\text{CO}_2$ was only observed at 48 and 96 hpf, and not at 30 hpf (this
473 study).

474 As well as directly causing shell dissolution, a number of other biological processes
475 responsible for larval shell calcification, such as matrix protein production, chitin
476 synthesis and enzymatic control are influenced by changes in seawater $p\text{CO}_2$ (Weiss et
477 al., 2013). For example, the activity of carbonic anhydrase, an enzyme that catalyzes the
478 reversible hydration of CO_2 to HCO_3^- and H^+ , reaches its maximum activity at the end
479 of each developmental stage and has been correlated with larval shell biomineralization

480 (Gaume et al., 2011; Medakovic, 2000). In the mussel *M. edulis*, six months of
481 incubation at 750 μatm $p\text{CO}_2$ (pH 7.5) significantly reduced carbonic anhydrase activity
482 within the mantle tissue, explaining shell growth reduction (Fitzer et al., 2014b). More
483 recently, evidence from proteomic studies suggests that elevated $p\text{CO}_2$ influences a
484 wide range of molecular pathways, including several associated with biomineralization,
485 metabolism and the cytoskeleton, and which may correlate with calcification
486 (Dineshram et al., 2015; Harney et al., 2016).

487 In order to discriminate between the effect of the aragonite saturation state and the
488 complex physiological effects of pH decrease on mollusk shell formation, future studies
489 should explicitly consider CaCO_3 saturation state in experimental seawater and the ability
490 of the species to maintain internal pH at the site of calcification. Failure to properly
491 biomineralise at this early stage not only results in reduced survival and developmental
492 problems for larvae (Byrne, 2012), but can also have carry-over effects later in life
493 (Hettinger et al., 2013; Rühl et al., 2017), which can explain why larval stages represent
494 such a major bottleneck for population persistence under changing environmental
495 conditions (Przeslawski et al., 2015). In this study, fertilization was carried out under
496 ambient conditions, and resulting embryos were transferred into experimental tanks
497 with different $p\text{CO}_2$ conditions, as is the case of most studies assessing the impacts of
498 ocean acidification on mollusk larvae. It is now well established that exposure of adults
499 to elevated CO_2 during reproductive conditioning can result in positive or negative
500 carry-over effects being transmitted from adults to their offspring, influencing the
501 resilience of mollusks to ocean acidification (Fitzer et al., 2014; Parker et al., 2013). In
502 the oyster *S. glomerata*, Parker et al. (2012) found that larvae from parents exposed to
503 elevated CO_2 during reproductive conditioning were larger and developed faster when
504 they also experienced reduced pH, as compared to larvae from parents conditioned

under ambient pH. These results highlight the importance of assessing carry-over effects for determining species responses to ocean acidification. To overcome this problem, future projects should conduct long-term transgenerational experiments. Biological responses measured during long-term exposure to elevated $p\text{CO}_2$, from reproducing adults to larval and juvenile stages, will provide valuable information regarding acclimation and adaptation of abalone to changing ocean conditions. In addition, the exploration of multiple stressors known to interact with pH (e.g. temperature, salinity, pathogens and pollutants) will result in more ecologically realistic simulations of the impact of global environmental change, providing a greater understanding of ecological relationships (e.g. Ko et al., 2014). Indeed, consideration of multiple stressors is also crucial in fisheries and aquaculture to identify optimal conditions and adapt culturing practices for sustainable shellfish production.

517

518 **Acknowledgements**

519 N. Wessel was supported by a post-doctoral fellowship from the MNHN (Ministère
520 de l'Enseignement Supérieur et de la Recherche, Paris, France). This work was financed
521 in part by the ATM program “Biomineralisation” of the MNHN funded by the Ministère
522 délégué à l'Enseignement Supérieur et à la Recherche (Paris, France). V. Julia, F. Nunes
523 and E. Harney were supported by a grant from the Regional Council of Brittany, from
524 the European Funds (ERDF) and supported by the “Laboratoire d'Excellence”
525 LabexMER (ANR-10-LABX-19) and co-funded by a grant from the French government
526 under the program “Investissements d'Avenir”. We thank Gérard Sinquin for his
527 assistance in scanning electron microscopy (Plateforme d'Imagerie et de Mesures en
528 Microscopie, Université de Bretagne Occidentale, Brest). P. Dubois is a Research
529 Director of the National Fund for Scientific Research (Belgium).

530 The experiments complied with the current French laws.

531 **Figures and tables**

532 **Figure 1.** Trochophore larvae grown in control condition (A) and at pH 7.6 (B). These
533 larvae were respectively classified in the morphological groups 1 (normal shelled) and 3
534 (unshelled larval phenotype). s: shell, pt: prototrochal ciliary band, at: apical tuft.
535 Dotted black arrows indicate the length and width measurements.

536

537 **Figure 2.** Morphological variables measured in abalone veliger larvae grown in various
538 pH conditions; the group in brackets refers to morphological groups described in section
539 2.3.2. **A:** 30 hpf at pH 8.0 (group 1), **B:** 30 hpf at pH 7.6 (group 2), **C:** 30 hpf at pH 7.6
540 (group 4). **D:** 48 hpf at pH 8.0 (group 1), **E:** 48 hpf at pH 7.6 (group 2), **F:** 48 hpf at
541 pH 7.6 (group 4). **G:** 96 hpf at pH 8.0 (group 1), **H:** 96 hpf at pH 7.6 (group 3), **I:**
542 96 hpf at pH 7.6 (group 4). Arrows indicate attributes: eyes (e), foot (f), mantle (m),
543 shell (s); arrowheads indicate shell abnormalities (sa) or deformed shell (ds); dotted
544 arrows indicate the length and width measurements.

545

546 **Figure 3.** Viability of abalone larvae exposed to different pH conditions at 30 hpf (light
547 grey), 48 hpf (grey) and 96 hpf (dark grey). Errors bars represent standard deviations.
548 Asterisks denote significant difference between control and low-pH condition (unpaired
549 Student's t-test, $p < 0.05$).

550

551 **Figure 4.** Morphology and development of abalone larvae exposed to different pH
552 conditions at 20 hpf (A), 30 hpf (B), 48 hpf (C), and 96 hpf (D). Grey levels represent
553 the morphological groups, according to the developmental stage. **A (trochophore**
554 **larvae):** black: normal shelled larvae; dark grey : shelled larvae with abnormalities or
555 delayed development; light grey: unshelled larvae with normal body; white: unshelled

556 larvae with abnormalities or delayed development; **B, C, D (veliger larvae)** : black:
557 normal shelled larvae; dark grey larvae with shell malformation(s)/ normal body; light
558 grey : shelled larvae with body abnormalities or delayed development; white: larvae
559 with both shell and body abnormalities.

560

561 **Figure 5.** Scanning electron microscopy (SEM) images of abalone larvae grown under
562 control (A, B) and low pH condition (C, D). Shell surfaces of 48 hpf veliger are shown.
563 **A:** lateral view of a 48h-old veliger under control pH (8.0); the protoconch is well
564 developed and covers almost completely the larval body; **B:** detail of the shell surface
565 boxed in 5A showing a uniform granular texture covered by a very thin organic coating;
566 **C:** lateral view of a 48h-old veliger exposed to low pH (7.6); the protoconch appears
567 well developed but exhibits an heterogeneous surface; **D:** detail of the protoconch
568 surface boxed in 5C showing numerous small holes interspaced between the
569 biominerals and remnants of the organic coating.

570

571 **Figure 6.** Correlation between length and width for each pH treatment. Light grey
572 represents the control pH (8.0), dark grey represents the pH 7.7, and black represents the
573 pH 7.6. Results of the statistical analyses are reported in Table 2.

574

575 **Figure 7.** Effect of decreased pH on abalone larval growth, expressed as square roots
576 of (length x width) at 20 hpf (A), 30 hpf (B), 48 hpf (C), and 96 hpf (D). Grey level of
577 the boxes denote the different pH conditions. Centre lines of box plots show the
578 medians; box limits indicate the first and third quartile respectively with lines
579 encompassing data within 1.5 times the spread from the median ($p < 0.05$). Results of
580 the statistical analyses are reported in Table 3.

581

582 **Figure 8.** Morphology and shell birefringence of 48 hpf veliger larvae grown under
583 control (A, B) and low pH conditions (C, D). Larvae were observed under phase
584 contrast (A, C) and polarized microscopy (B, D). Normal larvae under control pH (8.0)
585 showing the characteristic black cross of birefringence (A, B). Shell abnormalities in
586 larvae exposed to low pH (7.7) result in a significant decrease of calcified areas (C, D).

587

588 **Figure 9.** Shell mineralization of larval abalone determined by polarized light
589 microscopy for each development stage (A: 30hpf, B: 48hpf, C: 96hpf). Grey levels
590 represent the three categories of mineralization: black bars for fully mineralized
591 (birefringence > 90%); stripe bars for partially mineralized (70% < birefringence <
592 90%) and dotted bars for less mineralized shells (birefringence < 70%). Differences in
593 larval distribution across pH treatments were tested using a homogeneity χ^2 test by
594 treating birefringence as a categorical factor (n=40 larvae per pH condition). Results of
595 the statistical analyses are reported in Table 4.

596

597 **Table 1.** Mean parameters of seawater carbonate chemistry during the experiment.
598 Seawater pH on the total scale (pH_T), temperature ($17.0 \pm 0.5^\circ\text{C}$), salinity (37.0 ± 0.1)
599 and total alkalinity (mean $2344 \mu\text{Eq}.\text{kg}^{-1}$) were used to calculate CO_2 partial pressure
600 ($p\text{CO}_2$; μatm), Dissolved Inorganic Carbon (DIC; $\mu\text{mol}.\text{kg}^{-1}$ SW), HCO_3^- , CO_3^{2-} ,
601 aragonite saturation state (Ω_{ar}) and calcite saturation state (Ω_{calc}) by using the
602 CO_2SYS software. pH_T is the average value logged throughout the 5 days of experiment
603 (every 15 mn) in the two tanks ($n = 96/\text{tank}$). Temperature and salinity were measured
604 daily ($n = 5$); total alkalinity was measured twice ($n = 2$). Results are expressed as
605 mean \pm SD.

606

607

608 **Table 2:** Results of the Spearman's correlation performed to evaluate the nullity of
609 correlation between larval length and width for each pH treatment in the course of the
610 experiment.

611

612 **Table 3.** Summary of statistics used to test the differences in larval growth.

613 **A.** Results of the repeated measures ANOVA on larval growth index (square root of
614 length * width); **B.** Multiple comparison Tukey tests testing the effects of pH (fixed
615 crossed factor) according to time (fixed repeated factor). Significant results in bold ($p <$
616 0.05).

617

618 **Table 4.** Summary of statistics used to test the differences in shell birefringence.

619 **A.** Homogeneity χ^2 test used to test the effect of pH on shell birefringence, for each
620 development stage. **B.** Pair-wise Wilcoxon rank sum test showing differences between
621 pH groups; Bonferroni adjusted p -values. Significant results in bold ($p < 0,05$).

622

623 **Supplementary Figure S1.** **A.** Cross-polarized microscopy image of abalone larvae (48
624 hpf) showing the three regions of interest (ROI) selected for the analysis of
625 birefringence intensity. **B.** Quantification of grey-scale levels (in pixels) in the three
626 ROI. The values were averaged to provide a global mean grey level for each larval shell
627 ($n = 40$ larvae per pH condition).

628

630 **References**

- 631 Auzoux-Bordenave, S., Badou, A., Gaume, B., Berland, S., Helléouet, M.-N., Milet, C.,
632 and Huchette, S. 2010. Ultrastructure, chemistry and mineralogy of the growing
633 shell of the European abalone *Haliotis tuberculata*. J. Struct. Biol. 171: 277-290.
- 634 Byrne, M. 2012. Global change ecotoxicology: Identification of early life history
635 bottlenecks in marine invertebrates, variable species responses and variable
636 experimental approaches. Mar. Environ. Res. 76: 3-15.
- 637 Byrne, M., Ho, M., Wong, E., Soars, N. A., Selvakumaraswamy, P., Shepard-Brennand,
638 H., Dworjanyn, S. A., *et al.* 2011. Unshelled abalone and corrupted urchins:
639 development of marine calcifiers in a changing ocean. Proc. R. Soc. B: Biological
640 Sciences, 278: 2376-2383.
- 641 Comeau, S., Gorsky, G., Alliouane, S., and Gattuso, J.- P. 2010. Larvae of the pteropod
642 *Cavolinia inflexa* exposed to aragonite undersaturation are viable but shell-less.
643 Mar. Biol. 157: 2341-2345.
- 644 Cook, P. A. 2014. The Worldwide Abalone Industry. Modern Economy, 05: 1181-1186.
- 645 Courtois de Viçose, G., Viera, M. P., Bilbao, A., and Izquierdo, M. S. 2007. Embryonic
646 and larval development of *Haliotis tuberculata coccinea* Reeve: an indexed micro-
647 photographic sequence. J. Shellfish Res. 26: 847-854.
- 648 Crim, R. N., Sunday, J. M., and Harley, C. D. G. 2011. Elevated seawater CO₂
649 concentrations impair larval development and reduce larval survival in endangered
650 northern abalone (*Haliotis kamtschatkana*). J. Exp. Mar. Biol. Ecol. 400: 272-277.
- 651 Dickson, A.G., Sabine, C.L., Christian, J.R. (Eds), 2007. Guide to best practices for
652 ocean CO₂ measurements. PICES Special Publication, 3: 191 pp.
- 653 Dickson, A.G. 2010. The carbon dioxide system in seawater: equilibrium chemistry and
654 measurements. In Guide to Best Practices for Ocean Acidification Research and

- 655 Data Reporting pp.17-40. Ed. By U. Riebesell, V. J. Fabry, L. Hansson and J.-P.
656 Gattuso). Luxembourg: Publications Office of the European Union.
- 657 Dickson, A.G., and Millero, F.J. 1987. A comparison of the equilibrium constants for
658 the dissociation of carbonic acid in seawater media. Deep Sea Res. 34: 1733–1743.
- 659 Dineshram, R., Quan, Q., Sharma, R., Chandramouli, K., Yalamanchili, H.K., Chu, I.
660 and Thiagarajan, V., 2015. Comparative and quantitative proteomics reveal the
661 adaptive strategies of oyster larvae to ocean acidification. Proteomics 15, 4120–
662 4134.
- 663 Doncaster, C. P. and Davey, A. J. H. 2007. Analysis of Variance and Covariance: How
664 to Choose and Construct Models for the Life Sciences. Cambridge: Cambridge
665 University Press.
- 666 Ekstrom, J., Suatoni, L., Cooley, S., Pendleton, L., Waldbusser, G., Cinner, J., Ritter, J.,
667 Langdon, C., van Hooidonk, R., Gledhill, D., Wellman, K., Beck, M., Brander, L.,
668 Rittschof, D., Doherty, C., Edwards, P. & Portela, R. 2015. Vulnerability and
669 adaptation of US shellfisheries to ocean acidification. Nature Climate Change, 5:
670 207–214.
- 671 Ellis, R. P., Bersey, J., Rundle, S. D., Hall-Spencer, J. M., and Spicer, J. I. 2009. Subtle
672 but significant effects of CO₂ acidified seawater on embryos of the intertidal snail,
673 *Littorina obtusata*. Aquat. Biol. 5: 41-48.
- 674 Eyster, LS. 1986. Shell inorganic composition and onset of shell mineralization during
675 bivalve and gastropod embryogenesis. Biol. Bull. 170:211–231
- 676 Fitzer, S.C., Cusack, M., Phoenix, V.R., Kamenos, N.A. 2014. Ocean acidification
677 reduces the crystallographic control in juvenile mussel shells. J. Struct. Biol. 188 :
678 39-45.

- 679 Fitzer, S.C., Phoenix, V.R., Cusack, M., Kamenos, N.A. 2014b. Ocean acidification
680 impacts mussel control on biomineralisation. Sci. Rep. 4, 6218.
681 (doi:10.1038/srep06218).
- 682
- 683 Frieder, C.A., Applebaum, S.L., Pan, T.-C.F., Hedgecock, D. and Manahan, D.T., 2016.
684 Metabolic cost of calcification in bivalve larvae under experimental ocean
685 acidification. ICES J. Mar. Sci. 74: 941–954.
- 686 Gattuso, J. P., Magnan, A., Bille, R., Cheung, W. W. L., Howes, E. L., Joos, F.,
687 Allemand, D., *et al.* 2015. Contrasting futures for ocean and society from different
688 anthropogenic CO₂ emissions scenarios. Science 349: aac4722.
- 689 Gaume, B., Fouchereau-Peron, M., Badou, A., Hellouet, M.-N., Huchette, S., and
690 Auzoux-Bordenave, S. 2011. Biomineralization markers during early shell
691 formation in the European abalone *Haliotis tuberculata*, Linnaeus. Mar. Biol. 158:
692 341-353.
- 693 Gazeau, F., Gattuso, J. P., Dawber, C., Pronker, A. E., Peene, F., Peene, J., Heip, C. H.
694 R., *et al.* 2010. Effect of ocean acidification on the early life stages of the blue
695 mussel *Mytilus edulis*. Biogeosciences 7: 2051-2060.
- 696 Gazeau, F., Parker, L. M., Comeau, S., Gattuso, J.-P., O'Connor, W. A., Martin, S.,
697 Pörtner, H.-O., *et al.* 2013. Impacts of ocean acidification on marine shelled
698 mollusks. Mar. Biol. 160: 2207-2245.
- 699 Gazeau, F., Quiblier, C., Jansen, J. M., Gattuso, J.-P., Middelburg, J. J., and Heip, C. H.
700 R. 2007. Impact of elevated CO₂ on shellfish calcification. Geophys. Res. Lett. 34.
- 701 Guo, X., Huang, M., Pu, F., You, W., and Ke, C. 2015. Effects of ocean acidification
702 caused by rising CO₂ on the early development of three mollusks. Aquat. Biol. 23:
703 147-157.

- 704 Harney, E., Artigaud, S., Le Souchu, P., Miner, P., Corporeau, C., Essid, H., Pichereau,
705 V., *et al.* 2016. Non-additive effects of ocean acidification in combination with
706 warming on the larval proteome of the Pacific oyster, *Crassostrea gigas*. *J*
707 *Proteomics* 135: 151-161.
- 708 Hendriks, I. E., Duarte, C. M., and Álvarez, M. 2010. Vulnerability of marine
709 biodiversity to ocean acidification: A meta-analysis. *Estuar. Coast. Shelf. Sci.* 86:
710 157-164.
- 711 Hettinger, A., Sanford, E., Hill, T. M., Lenz, E. A., Russell, A. D., and Gaylord, B.
712 2013. Larval carry-over effects from ocean acidification persist in the natural
713 environment. *Glob. Change Biol.* 19, 3317–3326, doi: 10.1111/gcb.12307
- 714 Hofmann, G.E., Barry, J.P., Edmunds, P.J., Gates, R.D., Hutchins D.A., Klinger, T., and
715 Sewell, M.A. 2010. The effect of ocean acidification on calcifying organisms in
716 marine ecosystems: An organism-to-ecosystem perspective. *Annu. Rev. Ecol. Evol.*
717 *Syst.* 41: 127-147.
- 718 Huchette, S., and Clavier, J. 2004. Status of the ormer (*Haliotis tuberculata* L.) industry
719 in Europe. *J. Shellfish Res.* 23 : 951-955.
- 720 Hüning, A. K., Melzner, F., Thomsen, J. , Gutowska, M. A. , Krämer, L. , Frickenhaus,
721 S. , Rosenstiel, P. , Pörtner, H. O. , Philipp, E. E. R. and Lucassen, M. 2012.
722 Impacts of seawater acidification on mantle gene expression patterns of the Baltic
723 Sea blue mussel: implications for shell formation and energy supply. *Marine*
724 *Biology*. doi: 10.1007/s00227-012-1930-9
- 725 IPCC, 2014. Summary for Policymakers. In: Climate Change 2014: Impacts,
726 Adaptation, and Vulnerability. Part A: Global and Sectoral Aspects. Contribution of
727 Working Group II to the Fifth Assessment Report of the Intergovernmental Panel on
728 Climate Change. Cambridge University Press, Cambridge, United Kingdom and New
729 York, NY, USA, pp. 1-32.

- 730 Jardillier E., Rousseau M., Gendron-Badou A., Fröhlich F., Smith D.C., Martin M.,
731 Helléouet M.-N., Huchette S., Doumenc D., Auzoux-Bordenave S., 2008. A
732 morphological and structural study of the larval shell from the abalone *Haliotis*
733 *tuberculata*. Mar. Biol. 154 (4): 735-744.
- 734 Kimura, R. Y. O., Takami, H., Ono, T., Onitsuka, T., and Nojiri, Y. 2011. Effects of
735 elevated pCO₂ on the early development of the commercially important gastropod,
736 Ezo abalone *Haliotis discus hannai*. Fish. Oceanogr. 20: 357-366.
- 737 Ko, G., Dineshram, R., Campanati, C., Vera, S., Havenhand, J. & Thiagarajan, V.
738 2014. Interactive effects of ocean acidification, elevated temperature and reduced
739 salinity on early-life stages of the Pacific oyster. Environmental Science &
740 Technology, 48: 10079–10088.
- 741 Kroeker, K. J., Kordas, R. L., Crim, R. N., and Singh, G. G. 2010. Meta-analysis reveals
742 negative yet variable effects of ocean acidification on marine organisms. Ecol. Lett.
743 13: 1419-1434.
- 744 Kurihara, H. 2008. Effects of CO₂-driven ocean acidification on the early
745 developmental stages of invertebrates. Mar. Ecol. Prog. Ser. 373: 275-284.
- 746 Kurihara, H., Asai, T., Kato, S., and Ishimatsu, A. 2008. Effects of elevated pCO₂ on
747 early development in the mussel *Mytilus galloprovincialis*. Aquat. Biol. 4: 225-233.
- 748 Kurihara, H., Kato, S., and Ishimatsu, A. 2007. Effects of increased seawater pCO₂ on
749 early development of the oyster *Crassostrea gigas*. Aquat. Biol. 1: 91-98.
- 750 Lewis, E., and Wallace, D.W.R. 1998. Program developed for CO₂ system calculations.
751 Carbon Dioxide Information Analysis Center, Oak Ridge National Laboratory, U.S.
752 Department of Energy
- 753 Martin, S., Richier, S., Pedrotti, M. L., Dupont, S., Castejon, C., Gerakis, Y., Kerros, M.
754 E., *et al.* 2011. Early development and molecular plasticity in the Mediterranean sea

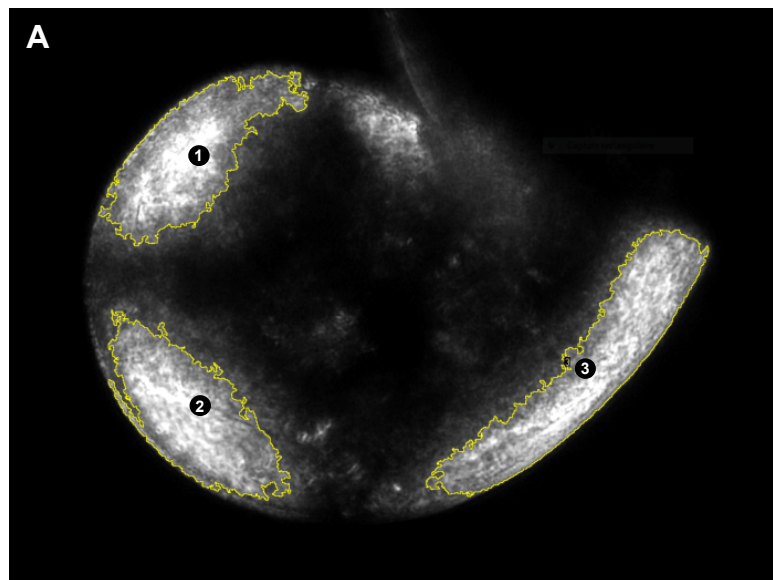
- 755 urchin *Paracentrotus lividus* exposed to CO₂-driven acidification. J. Exp. Biol. 214:
756 1357-1368.
- 757 Medakovic, D., 2000. Carbonic anhydrase activity and biomineralization process in
758 embryos, larvae and adult blue mussels *Mytilus edulis* L. Helgol Mar Res 54:1–6.
759 doi:10.1007/s101520050030
- 760 Mehrbach, C., Culberso, C., Hawley, J.E., and Pytkowic, R.M. 1973. Measurement of
761 apparent dissociation-constants of carbonic-acid in seawater at atmospheric pressure.
762 Limnol. Oceanogr. 18: 897–907.
- 763 Miller, A.W., Reynolds, A.C., Sobrino, C., and Riedel, G.F. 2009. Shellfish Face
764 Uncertain Future in High CO₂ World: Influence of Acidification on Oyster Larvae
765 Calcification and Growth in Estuaries. PLoS ONE 4(5): e5661.
766 doi:10.1371/journal.pone.0005661
- 767 Morash, A. J., and Alter K., 2015. Effects of environmental and farm stress on abalone
768 physiology: perspectives for abalone aquaculture in the face of global climate
769 change. Reviews in Aquaculture, (2015) 7, 1–27.
- 770 Noisette, F., Comtet, T., Legrand, E., Bordeyne, F., Davoult, D., and Martin, S. 2014.
771 Does Encapsulation Protect Embryos from the Effects of Ocean Acidification? The
772 example of *Crepidula fornicata*. PLoS ONE, 9: e93021.
- 773 Orr, J. C., Fabry, V. J., Aumont, O., Bopp, L., Doney, S. C., Feely, R. A.,
774 Gnanadesikan, A., *et al.* 2005. Anthropogenic ocean acidification over the twenty-
775 first century and its impact on calcifying organisms. Nature, 437: 681-686.
- 776 Pan, T.-C.F., Applebaum, S.L. and Manahan, D.T., 2015. Experimental ocean
777 acidification alters the allocation of metabolic energy. Proc. Natl. Acad. Sci. 112:
778 4696–4701.

- 779 Parker, L., Ross, P., O'Connor, W., Borysko, L., Raftos, D. & Pörtner, H. 2012. Adult
780 exposure influences offspring response to ocean acidification in oysters. *Glob. Change Biol.* 18: 82–92.
- 782 Parker, L., Ross, P., O'Connor, W., Pörtner, H., Scanes, E., and Wright, J. 2013.
783 Predicting the Response of Mollusks to the Impact of Ocean Acidification. *Biology*,
784 2: 651-692.
- 785 Parker, L. M., Ross, P. M., and O'Connor, W. A. 2009. The effect of ocean acidification
786 and temperature on the fertilization and embryonic development of the Sydney rock
787 oyster *Saccostrea glomerata* (Gould 1850). *Glob. Change Biol.* 15: 2123-2136.
- 788 Parker, L. M., Ross, P. M., and O'Connor, W. A. 2010. Comparing the effect of
789 elevated $p\text{CO}_2$ and temperature on the fertilization and early development of two
790 species of oysters. *Mar. Biol.* 157: 2435-2452.
- 791 Przeslawski, R., Byrne, M., and Mellin, C. 2015. A review and meta-analysis of the
792 effects of multiple abiotic stressors on marine embryos and larvae. *Glob. Change
793 Biol.* 21: 2122-2140.
- 794 R Development Core Team. 2014. R: A language and environment for statistical
795 computing. R Foundation for Statistical Computing, Vienna, Austria.
- 796 Ramesh, K., Hu, M.Y., Thomsen, J., Bleich, M. and Melzner, F., 2017. Mussel larvae
797 modify calcifying fluid carbonate chemistry to promote calcification. *Nat. Commun.* 8: 1–8.
- 799 Riebesell, U., Fabry, V. J., Hansson, L., and Gattuso, J.-P. 2010. Guide to Best Practices
800 for Ocean Acidification Research and Data Reporting (Publications Office of the
801 European Union).
- 802 Ross, P. M., Parker, L., O'Connor, W. A., and Bailey, E. A. 2011. The Impact of Ocean
803 Acidification on Reproduction, Early Development and Settlement of Marine
804 Organisms. *Water*, 3: 1005-1030.

- 805 Rühl, S., Calosi, P., Faulwetter, S., Keklikoglou, K., Widdicombe, S. and Queirós,
806 A.M., 2017. Long-term exposure to elevated pCO₂ more than warming modifies
807 early-life shell growth in a temperate gastropod. ICES J. Mar. Sci. 74: 1113–1124.
- 808 Talmage, S.C., and Gobler, C.J., 2009. The effects of elevated carbon dioxide
809 concentrations on the metamorphosis, size, and survival of larval hard clams
810 (*Mercenaria mercenaria*), bay scallops (*Argopecten irradians*), and Eastern oysters
811 (*Crassostrea virginica*). Limnol. Oceanogr. 54:2072–2080
- 812 Talmage, S. C., and Gobler, C.J. 2010. Effects of past, present and future ocean carbon
813 dioxide concentrations on the growth and survival of larval shellfish. Proc. Natl.
814 Acad. Sci. USA 107: 17246–172.
- 815 Thomsen, J., Haynert, K., Wegner, K. M., and Melzner, F., 2015. Impact of seawater
816 carbonate chemistry on the calcification of marine bivalves. Biogeosciences, 12,
817 4209–4220,.
- 818 Timmins-Schiffman, E., O'Donnell, M. J., Friedman, C.S., and Roberts, S. B. 2013.
819 Elevated *pCO₂* causes developmental delay in early larval Pacific oysters,
820 *Crassostrea gigas*. Mar. Biol. 160: 1973-1982.
- 821 Travers, M.-A., Basuyaux, O., Le Goïc, N., Huchette, S., Nicolas, J.-L., Koken, M., and
822 Paillard, C. 2009. Influence of temperature and spawning effort on *Haliotis*
823 *tuberculata* mortalities caused by *Vibrio harveyi*: an example of emerging vibriosis
824 linked to global warming. Glob. Change Biol. 15: 1365-1376.
- 825 Waldbusser, G.G., Hales, B., Langdon, C. J., Haley, B. A., Schrader, P., Brunner, E. L.,
826 Gray, W. P., *et al.* 2015. Saturation-state sensitivity of marine bivalve larvae to
827 ocean acidification. Nat. Clim. Change 5:273–280.

- 828 Watson, S.-A., Southgate, P. C., Tyler, P. A., and Peck, L. S. 2009. Early Larval
829 Development of the Sydney Rock Oyster *Saccostrea glomerata* Under Near-Future
830 Predictions of CO₂-Driven Ocean Acidification. J. Shellfish Res. 28: 431-437.
- 831 Weiss, I.M., Lüke, F., Eichner, N., Guth, C and Clausen-Schaumann, H., 2013. On the
832 function of chitin synthase extracellular domains in biomineralization. J. Struct.
833 Biol. 183 (2): 216-225.
- 834 Widdicombe, S., and Spicer, J. I. 2008. Predicting the impact of ocean acidification on
835 benthic biodiversity: What can animal physiology tell us? J. Exp. Mar. Biol. Ecol.
836 366: 187-197.
- 837 Wittmann, A.C., and Pörtner, H-O. 2013. Sensitivities of extant animal taxa to ocean
838 Acidification. Nat. Clim. Change 3: 995–1001.
- 839 Zippay, M.L., and Hofmann, G.E. 2010. Effect of pH on gene expression and thermal
840 tolerance of early life history stages of red abalone *Haliotis rufescens*. J. Shellfish
841 Res. 29: 429-439.

Supplementary Figure S1:



B

ROI	Grey-scale level
1	97,977
2	98,022
3	100,713
Mean	98,90
SD	1,28

Figure 1

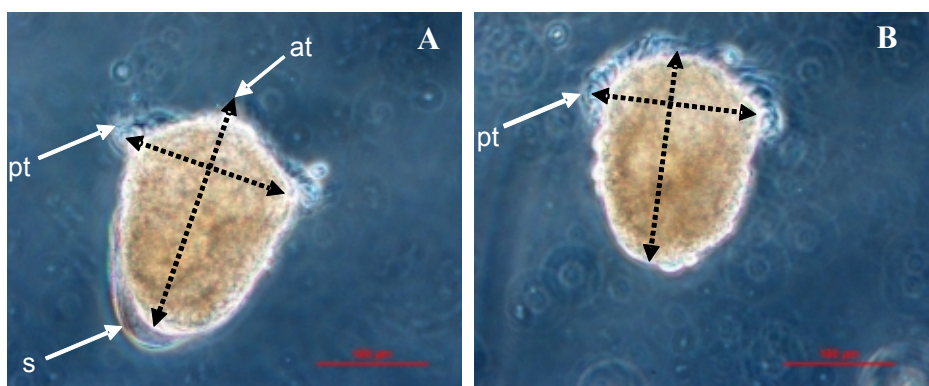


Figure 2

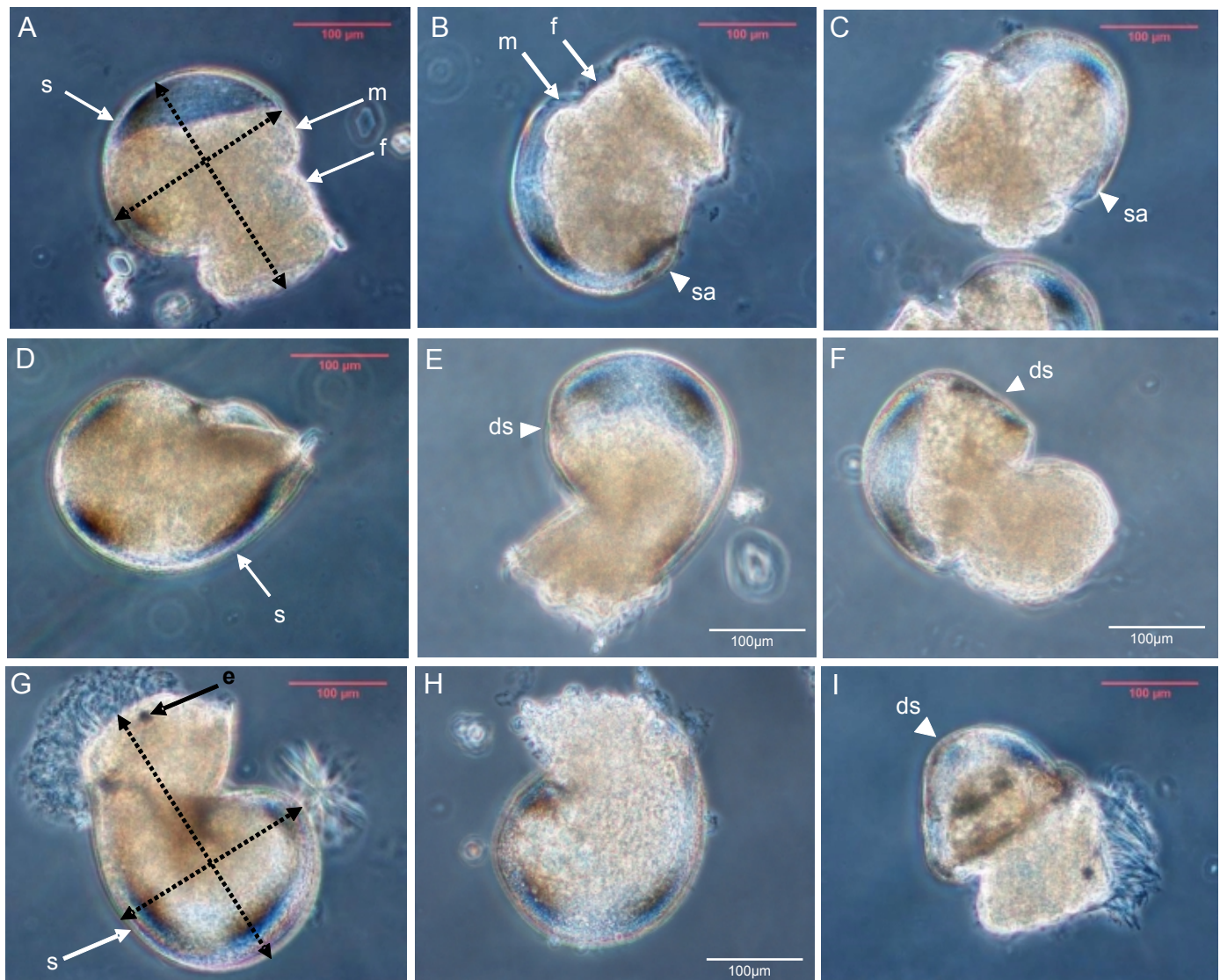


Figure 3

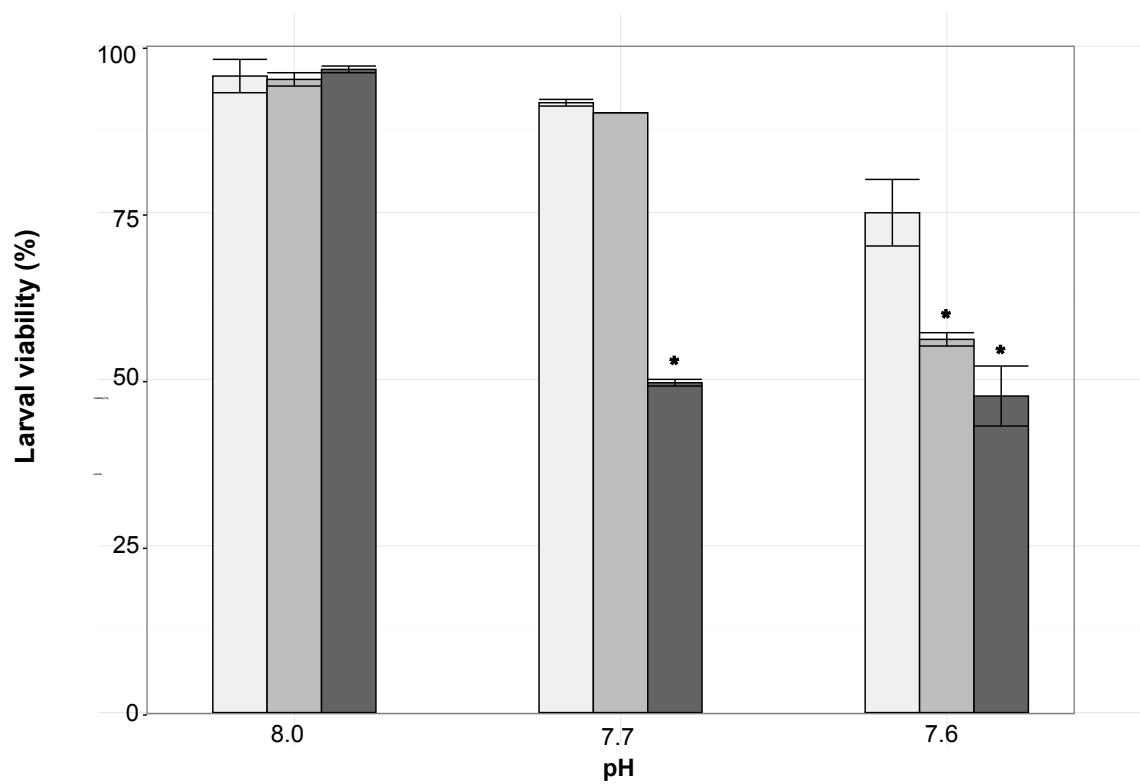


Figure 4

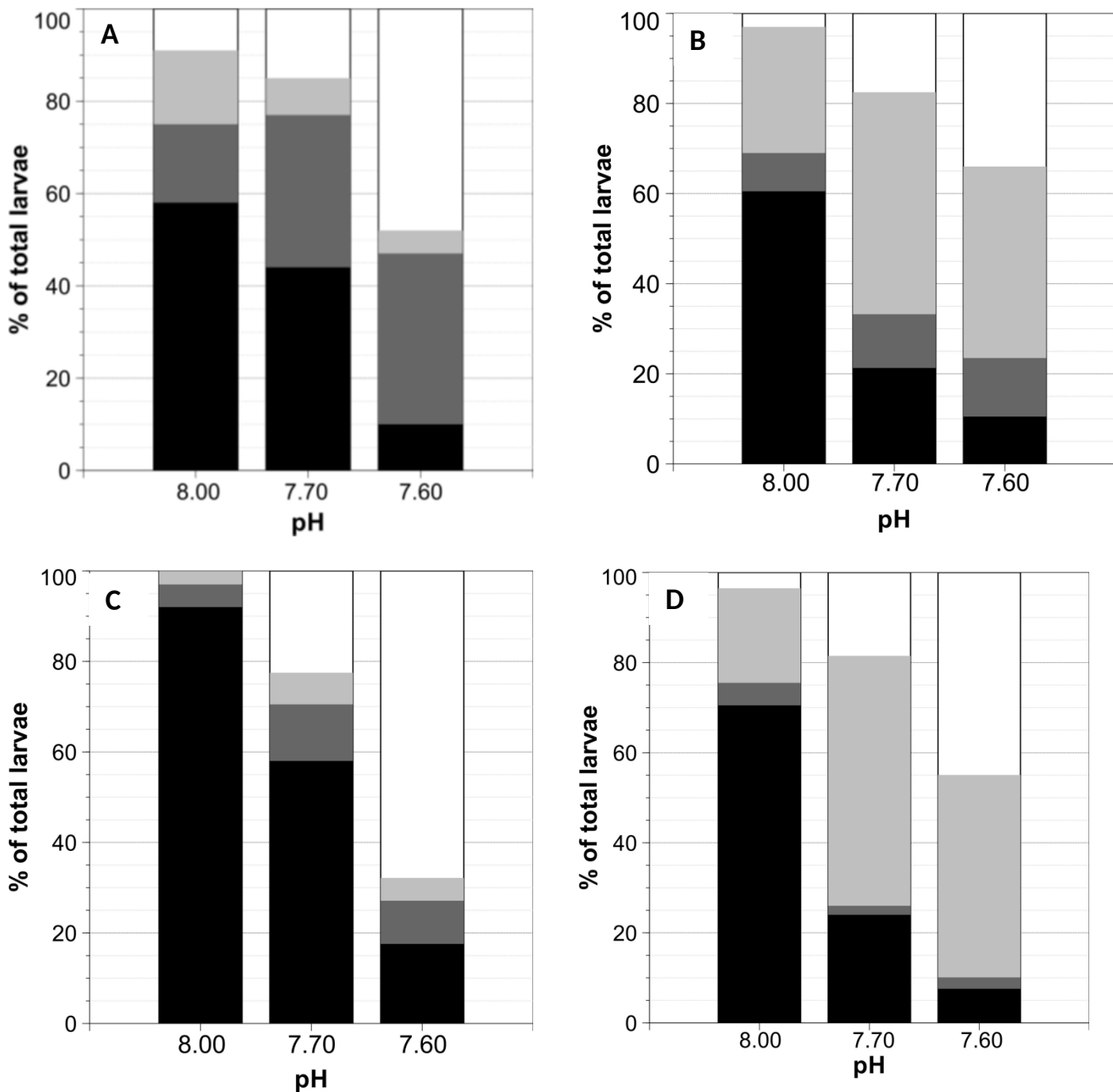


Figure 5

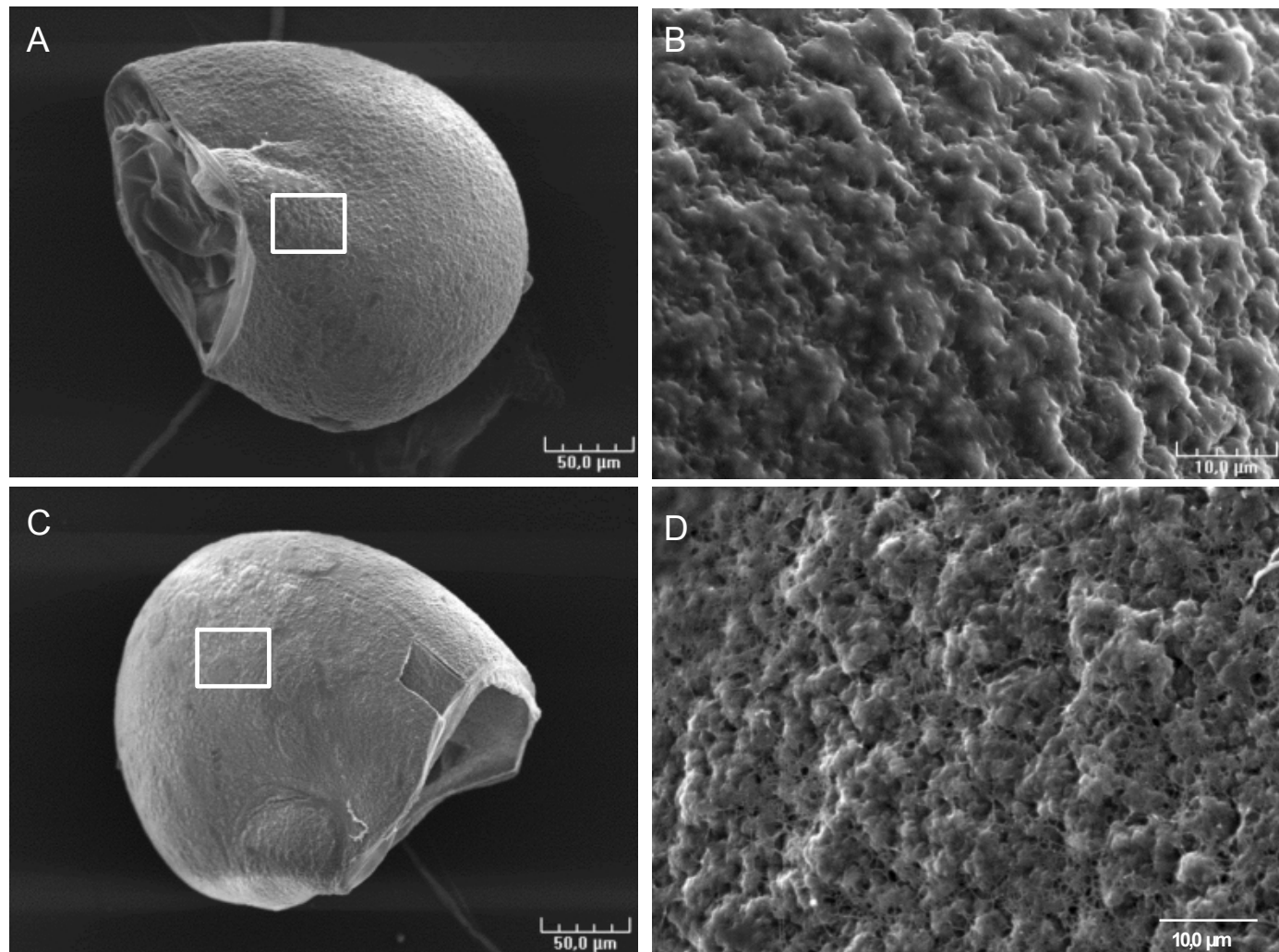


Figure 6

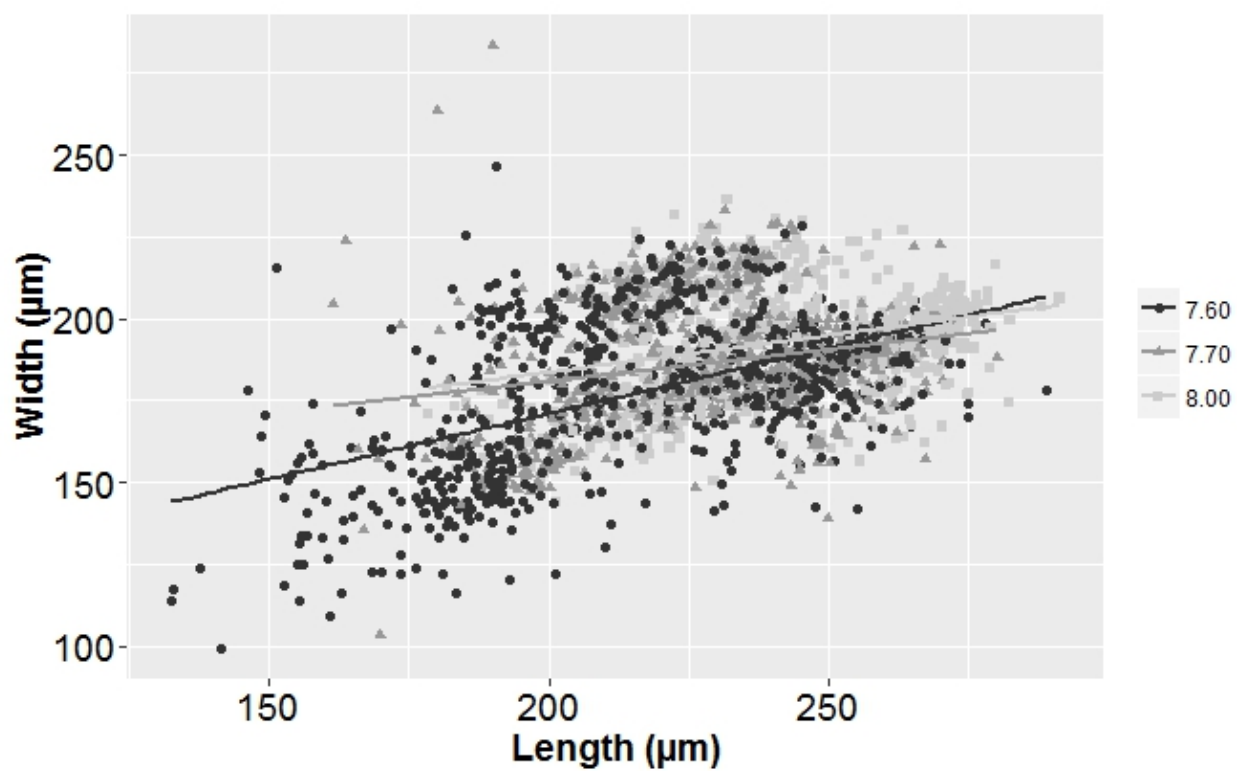


Figure 7

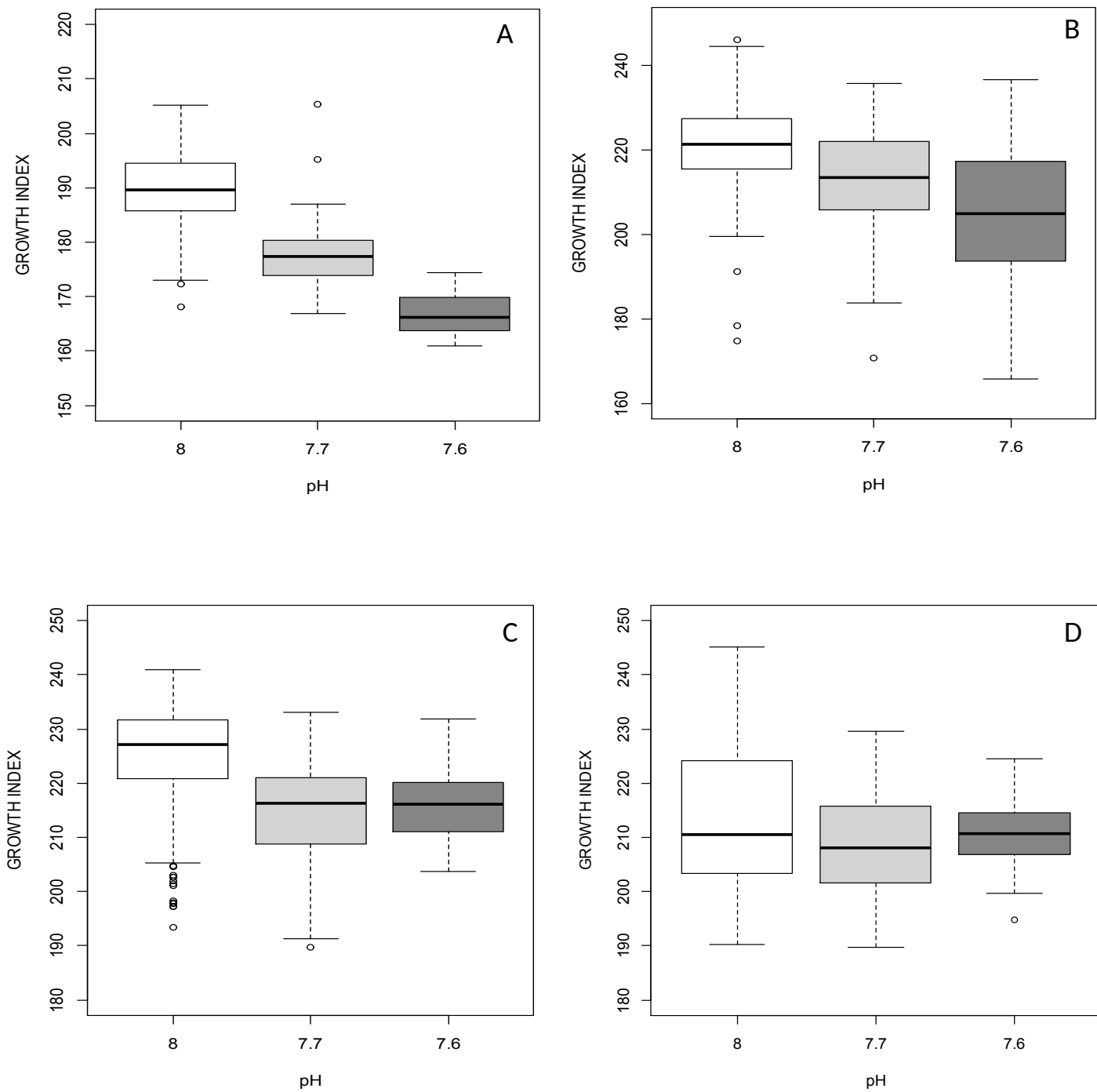


Figure 8

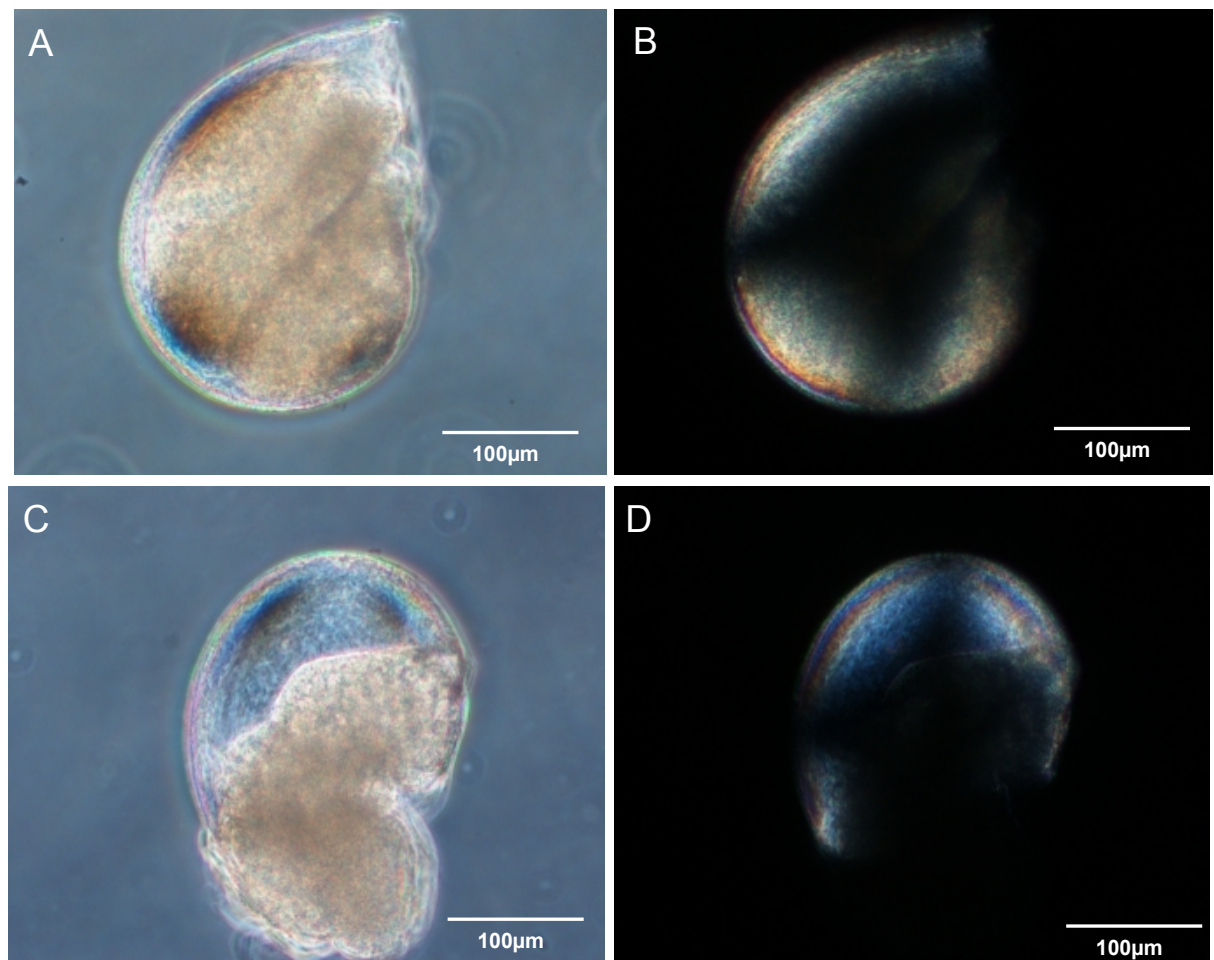


Figure 9

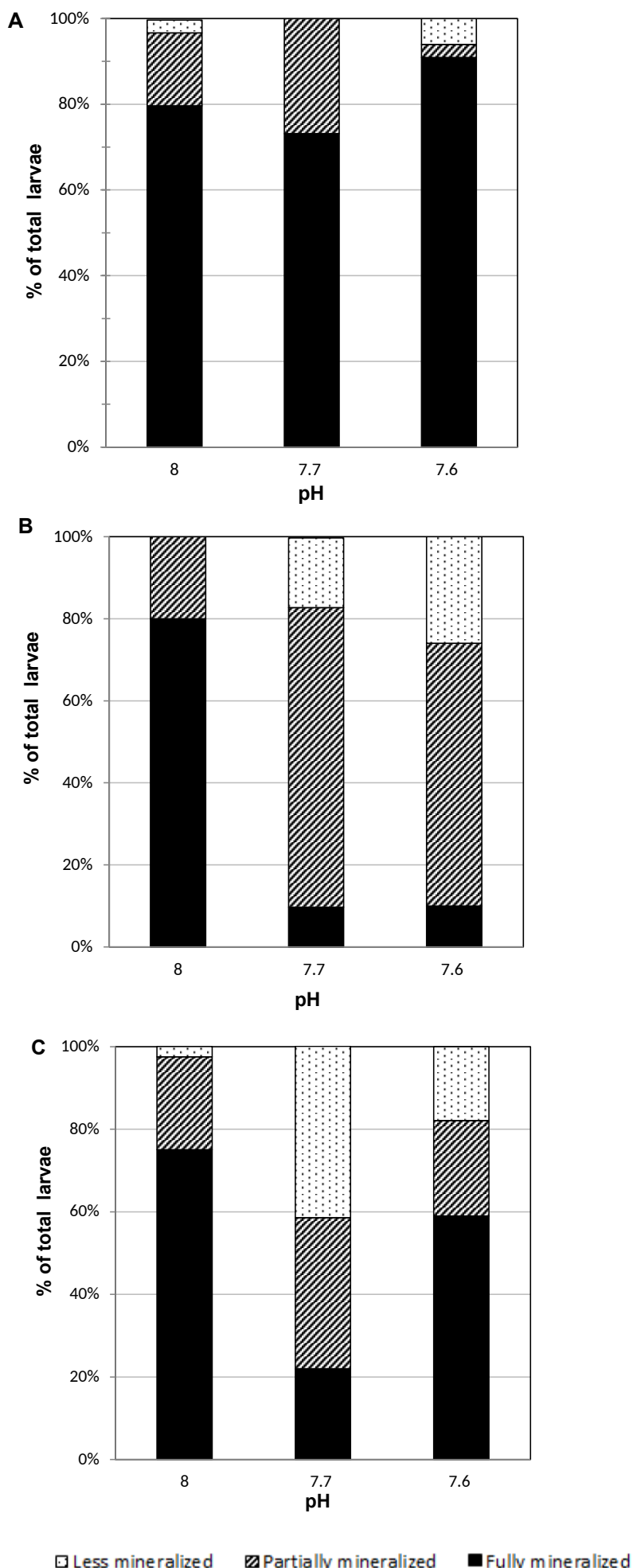


Table 1.

Nominal pH	pHT	pCO ₂ (μatm)	DIC (μmol/kg ⁻¹)	HCO ₃ ⁻ (μmol/kg ⁻¹)	CO ₃ ²⁻ (μmol/kg ⁻¹)	Ω ar	Ω calc
8.1	8.00 ± 0.002	460 ± 3	2119 ± 2	1940 ± 3	163 ± 1	2,47 ± 0,01	3,8 ± 0,02
7.7	7.68 ± 0,001	1055 ± 3	2254 ± 1	2132 ± 0,05	85,4 ± 0,3	1,30 ± 0,01	2 ± 0,01
7.6	7.58 ± 0,003	1331 ± 10	2286 ± 2	2170 ± 2	70,1 ± 0,6	1,06 ± 0,01	1,6 ± 0,01

Table 2.

Treatment (pH)	Rho	p-value
8.0	0.2842896	<0.001
7.7	0.1919181	<0.001
7.6	0.4593034	<0.001

Table 3.**A. Repeated measures ANOVA**

Effect between subjects	df	MS	F-ratio	p-value
pH	2	357.3	33.1	0.009
Error	3	10.8		
Effect within subjects	df	MS	F-ratio	p-value
Time	3	1998	141.6	<0.001
Time * pH	6	38.0	2.7	0.088
Error	9	14.1		

B. Multiple comparisonson factor time: *p*-value

20h vs 30h	0.002
20h vs 48h	<0.001
20h vs 96h	<0.001
30h vs 48h	0.159
30h vs 96h	0.418
48h vs 96h	0.009

on factor pH: *p*-value

7.6 vs 7.7	0.105
7.6 vs 8.0	0.008
7.7 vs 8.0	0.031

Table 4.**A. Homogeneity χ^2 test**

Development Time	Chi-sq	df	p-value
30h	9.28	4	0.055
48h	67.53	4	<0.001
96h	28.48	4	<0.001

B. Pair wise Wilcoxon rank sum test

pH factor	48h	96h
	p-value	p-value
7.7 vs 8.0	<0.001	<0.001
7.6 vs 8.0	<0.001	0.073
7.6 vs 7.7	0.49	0.0016